doi:10.1093/brain/aws177 Brain 2012: 135; 2428–2439 | 2428

BRAIN
A JOURNAL OF NEUROLOGY

Calpastatin-mediated inhibition of calpains in the mouse brain prevents mutant ataxin 3 proteolysis, nuclear localization and aggregation, relieving Machado–Joseph disease

Ana T. Simões,[1,2] Nélio Gonçalves,[1,2] Arnulf Koeppen,[3] Nicole Déglon,[4] Sebastian Kügler,[5] Carlos Bandeira Duarte[1,6] and Luís Pereira de Almeida[1,2]

1 Centre for Neuroscience and Cell Biology, University of Coimbra, 3004-517 Coimbra, Portugal
2 Faculty of Pharmacy, University of Coimbra, 3000-548 Coimbra, Portugal
3 VA Medical Centre and Albany Medical College, Albany, NY 12208, USA
4 Department of Clinical Neurosciences, Laboratory of Cellular and Molecular Neurotherapies, Lausanne University Hospital, Lausanne 1011, Switzerland
5 Department of Neurology, Vector Laboratory, University of Göttingen, 37073 Göttingen, Germany
6 Department of Life Sciences, Faculty of Sciences and Technology, University of Coimbra, 3001-401 Coimbra, Portugal

Correspondence to: Luís Pereira de Almeida, PhD
Centre for Neuroscience and Cell Biology,
University of Coimbra,
Largo Marquês de Pombal,
3004-517 Coimbra,
Portugal
E-mail: luispa@ci.uc.pt or luispa@cnc.uc.pt

Machado–Joseph disease is the most frequently found dominantly-inherited cerebellar ataxia. Over-repetition of a CAG trinucleotide in the *MJD1* gene translates into a polyglutamine tract within the ataxin 3 protein, which upon proteolysis may trigger Machado–Joseph disease. We investigated the role of calpains in the generation of toxic ataxin 3 fragments and pathogenesis of Machado–Joseph disease. For this purpose, we inhibited calpain activity in mouse models of Machado–Joseph disease by overexpressing the endogenous calpain-inhibitor calpastatin. Calpain blockage reduced the size and number of mutant ataxin 3 inclusions, neuronal dysfunction and neurodegeneration. By reducing fragmentation of ataxin 3, calpastatin overexpression modified the subcellular localization of mutant ataxin 3 restraining the protein in the cytoplasm, reducing aggregation and nuclear toxicity and overcoming calpastatin depletion observed upon mutant ataxin 3 expression. Our findings are the first *in vivo* proof that mutant ataxin 3 proteolysis by calpains mediates its translocation to the nucleus, aggregation and toxicity and that inhibition of calpains may provide an effective therapy for Machado–Joseph disease.

Keywords: Machado–Joseph disease; spinocerebellar ataxia type 3; proteolysis; calpastatin; cleavage fragment

Abbreviations: AAV = adeno-associated virus; DARPP-32 = dopamine- and cyclic AMP-regulated neuronal phosphoprotein; GFP = green fluorescent protein

Received January 16, 2012. Revised April 26, 2012. Accepted May 25, 2012

Introduction

Machado–Joseph disease, also known as spinocerebellar ataxia type 3, was originally described in people of Portuguese descent and is now considered to be the most frequent form of the autosomal dominantly inherited cerebellar ataxias. Machado–Joseph disease is a neurodegenerative disorder characterized by abnormal movement (Sudarsky and Coutinho, 1995) and is caused by an unstable and expanded polyglutamine repeat of >55 CAGs within the coding region of the causative gene, *MJD1*, on chromosome 14q32.1 (Kawaguchi *et al*., 1994), conferring a toxic gain of function to the ubiquitin-binding protein ataxin 3 (*ATXN3*) (Rubinsztein *et al*., 1999; Wang *et al*., 2000; Burnett *et al*., 2003; Doss-Pepe *et al*., 2003; Scheel *et al*., 2003; Chai *et al*., 2004).

Ataxin 3 is a protein of ~42 kDa and is predominantly expressed cytoplasmatically (Paulson *et al*., 1997*a*; Schmidt *et al*., 1998), even though it is small enough to enter the nucleus through passive diffusion (Marfori *et al*., 2011). Upon polyglutamine expansion, in spite of the increase in its molecular weight which could hinder access to the nucleus, mutant ataxin 3 accumulates in ubiquitinated intranuclear inclusions (Paulson *et al*., 1997*b*). The toxic fragment hypothesis predicts that proteolytic cleavage of the full-length polyglutamine protein initiates the aggregation process associated with inclusion formation and cellular dysfunction (Haacke *et al*., 2006; Takahashi *et al*., 2008).

A toxic cleavage fragment of mutant ataxin 3 was first proposed to trigger neurodegeneration by Ikeda *et al*. (1996). Indeed, the C-terminal fragment of mutant ataxin 3 is more toxic than the full-length protein (Ikeda *et al*., 1996; Paulson *et al*., 1997*b*; Goti *et al*., 2004). Understanding the proteolytic mechanism involved and the cellular protease(s) responsible could unravel the trigger mechanism for Machado–Joseph disease and reveal potential targets for therapy. Haacke and colleagues observed in cell lysates that upon calcium influx, ataxin 3 was proteolysed by calpains in fragments that could escape cytoplasmic quality control (Haacke *et al*., 2007; Breuer *et al*., 2010). This observation was recently confirmed in patient specific induced pluripotent stem cell-derived neurons (Koch *et al*., 2011). Calpain regulation is therefore critical and can come about by binding to calpastatin, the only endogenous calpain-specific inhibitor identified thus far (Takano *et al*., 2005). How ataxin 3 cleavage fragments mediate neurotoxicity has not been evaluated in animal models of Machado–Joseph disease. Overactivation of calpains may contribute decisively to the pathology by increasing cleavage of ataxin 3 into fragments containing the expanded polyglutamine segment, which may be able to penetrate the nuclear pore, accumulate in the nucleus and induce neurodegeneration.

Herein, taking advantage of adeno-associated (AAV) viral vectors for overexpression of calpastatin, we set out to investigate in a lentiviral mouse model of Machado–Joseph disease (Alves *et al*., 2008) and transgenic mice overexpressing calpastatin (Takano *et al*., 2005) whether and how calpains are involved in the pathogenesis of the disease. We provide *in vivo* evidence that: (i) proteolysis by calpains is required for nuclear localization of mutant ataxin 3; (ii) inhibition of calpains significantly decreases neuronal dysfunction and neurodegeneration in a mouse model of Machado–Joseph disease; (iii) production of mutant ataxin 3 cleavage fragments and the resulting nuclear localization inversely correlate with calpastatin levels in a dose-dependent manner; and (iv) calpastatin is depleted from neurons bearing mutant ataxin 3 intranuclear inclusions. In conclusion, we provide new insights into mutant ataxin 3 proteolysis, nuclear translocation and a resulting role in the pathogenesis of Machado–Joseph disease, which indicate that calpain inhibition may provide a new avenue of therapy.

Materials and methods

Animals

Four-week-old C57BL/6J mice (Charles River) were used. The animals were housed in a temperature-controlled room maintained on a 12 h light/12 h dark cycle. Food and water were provided *ad libitum*. The experiments were carried out in accordance with the European Community directive (86/609/EEC) for the care and use of laboratory animals. The researchers received adequate training (Felasa-certified course) and certification to perform the experiments from the Portuguese authorities (Direcção Geral de Veterinária).

Human brain tissue

Post-mortem human brain tissue from dentate nucleus was obtained from the tissue donation program of the National Ataxia Foundation, Minneapolis, MN, USA (VA Medical Centre and Albany Medical College). The tissues included a control patient (female, 36 years) and three patients with Machado–Joseph disease: Patient O (female, 70 years, 67/23 CAG repeats); Patient W (female, 62 years, 74/22 CAG repeats); and Patient K (male, 53 years, 69/23 CAG repeats).

Machado–Joseph disease transgenic mice tissue

Cerebella of Machado–Joseph disease transgenic mice (5.5 and 15 weeks old, $n = 2$ and $n = 4$, respectively) (Torashima *et al*., 2008; Oue *et al*., 2009) expressing a truncated form of human ataxin 3 with 69 CAG repeats, and wild-type mice ($n = 3$; 20 weeks old) of an older offspring were dissected and treated for western blot analysis.

Production of viral vectors

Lentiviral vectors encoding human wild-type ataxin 3 (ATX-3 27Q) or mutant ataxin 3 (ATX-3 72Q) (Alves *et al*., 2008) were produced in 293T cells with a four-plasmid system, as previously described (de Almeida *et al*., 2001). The lentiviral particles were resuspended in 1% bovine serum albumin in PBS. The viral particle content of batches was determined by assessing HIV-1 p24 antigen levels (Retro Tek, Gentaur). Viral stocks were stored at −80°C.

AAV vectors were produced as previously described (Zolotukhin *et al*., 1999; Kugler *et al*., 2003).

In vivo injection into the striatum

Concentrated viral stocks were thawed on ice. Lentiviral vectors encoding human wild-type (ATX-3 27Q) or mutant ataxin 3 (ATX-3 72Q) were stereotaxically injected into the striatum at the following

coordinates: antero-posterior: +0.6 mm; lateral: ±1.8 mm; ventral: −3.3 mm; tooth bar: 0. Animals were anaesthetized by administration of avertin (10 μl/g intraperitoneally).

Wild-type and transgenic mice overexpressing calpastatin received a single 1 μl injection of 0.2 mg p24/ml lentivirus in each side: left hemisphere (ATX-3 27Q) and right hemisphere (ATX-3 72Q). Wild-type mice were co-injected with 1 μl of 0.4 mg p24/ml ataxin 3 72Q lentivirus and 3 μl of AAV1/2-green fluorescent protein (AAV1/2-GFP; left hemisphere) or AAV2-calpastatin (AAV2-CAST; right hemisphere).

For the western blot procedure, transgenic mice overexpressing calpastatin received a single 2 μl injection of 0.3 mg p24/ml lentivirus in each side: left hemisphere (ATX-3 27Q) and right hemisphere (ATX-3 72Q). Wild-type mice were co-injected with 1 μl of 0.6 mg of p24/ml ATX-3 72Q lentivirus and 4 μl of AAV1/2-GFP (left hemisphere) or AAV2-CAST (right hemisphere).

Mice were kept in their home cages for 4, 5 or 8 weeks before being sacrificed for immunohistochemical or western blot analysis.

Imunohistochemical procedure

After an overdose of avertin (2.5 times, 12 μl/g given intraperitoneally), transcardial perfusion of the mice was performed with a phosphate solution followed by fixation with 4% paraformaldehyde. The brains were removed and post-fixed in 4% paraformaldehyde for 24 h and cryoprotected by incubation in 25% sucrose/phosphate buffer for 48 h. The brains were frozen and 25 μm coronal sections were cut using a cryostat (LEICA CM3050 S) at −21°C. Slices throughout the entire striatum were collected in anatomical series and stored in 48-well trays as free-floating sections in PBS supplemented with 0.05 μM sodium azide. The trays were stored at 4°C until immunohistochemical processing.

Sections from injected mice were processed with the following primary antibodies: a mouse monoclonal anti-ataxin 3 antibody (1H9; 1:5000; Chemicon), recognizing the human ataxin 3 fragment from amino acids F112 to L249; a rabbit polyclonal anti-ubiquitin antibody (Dako, 1:1000); a mouse monoclonal anti-myc tag antibody, clone 4A6 (1:1000; Upstate, Cell Signalling Solutions); and a rabbit anti-dopamine- and cyclic AMP-regulated neuronal phosphoprotein (DARPP-32) antibody (1:1000; Chemicon), followed by incubation with the respective biotinylated secondary antibodies (1:200; Vector Laboratories). Bound antibodies were visualized using the VECTASTAIN® ABC kit, with 3,3′-diaminobenzidine tetrahydrochloride (DAB metal concentrate; Pierce) as substrate.

Double stainings for ataxin 3 (1H9; 1:3000), nuclear marker [DAPI (4′,6-diamidino-2-phenylindole), blue] and ubiquitin (Dako, 1:1000) or calpastatin (H300, 1:250, Santa Cruz) were performed. Free-floating sections from injected mice were incubated at room temperature for 2 h in PBS/0.1% Triton™ X-100 containing 10% normal goat serum (Gibco), and then overnight at 4°C in blocking solution with the primary antibodies. Sections were washed three times and incubated for 2 h at room temperature with the corresponding secondary antibodies coupled to fluorophores (1:200, Molecular Probes) diluted in the respective blocking solution. The sections were washed three times and then mounted in FluorSave™ Reagent (Calbiochem) on microscope slides.

Staining was visualized using Zeiss Axioskop 2 plus, Zeiss Axiovert 200 and Zeiss LSM 510 Meta imaging microscopes (Carl Zeiss Microimaging), equipped with AxioCam HR colour digital cameras (Carl Zeiss Microimaging) using 5×, 20×, 40× and 63× Plan-Neofluar and a 63× Plan/Apochromat objectives and the AxioVision 4.7 software package (Carl Zeiss Microimaging).

Quantitative analysis of fluorescence was performed with a semi-automated image-analysis software package (ImageJ software).

Cresyl violet staining

Coronal 25 μm thick striatal sections were cut using a cryostat. Pre-mounted sections were stained with cresyl violet for 30 s, differentiated in 70% ethanol, dehydrated by passing twice through 95% ethanol, 100% ethanol and xylene solutions and mounted onto microscope slides with Eukitt® (Sigma).

Evaluation of the volume of the dopamine- and cAMP-regulated neuronal phosphoprotein depleted volume

The extent of ataxin 3 lesions in the striatum was analysed by photographing, with a 1.25× objective, eight DARPP-32 stained sections per animal (25 μm thick sections at 200 μm intervals), selected to obtain complete rostrocaudal sampling of the striatum, and by quantifying the area of the lesion with a semi-automated image analysis software package (ImageJ). The volume was then estimated with the following formula: volume = $d(a_1 + a_2 + a_3 \ldots)$, where d is the distance between serial sections (200 μm) and $a_1 + a_2 + a_3$ are DARPP-32 depleted areas for individual serial sections (de Almeida *et al*., 2002).

Cell counts and morphometric analysis of ataxin 3 and ubiquitin inclusions

Coronal sections showing complete rostrocaudal sampling (one of eight sections) of the striatum were scanned with a 20× objective. The analysed areas of the striatum encompassed the entire region containing ataxin 3 and ubiquitin inclusions, as revealed by staining with the anti-ataxin 3 and anti-ubiquitin antibodies. All inclusions were manually counted using a semiautomated image-analysis software package (ImageJ). Inclusions diameter was assessed by scanning the area above the needle tract in four different sections, using a 63× objective. At least 100 inclusions showing double staining for mutant ataxin 3 and GFP or calpastatin were analysed using LSM Image Browser.

Western blot analysis

For assessment of ataxin 3 proteolysis in the lentiviral model of Machado–Joseph disease, transcardial perfusion of the mice was performed with ice-cold PBS containing 10 mM EDTA (ethylenediaminetetraacetic acid) and 10 mM of the alkylating reagent *N*-ethylmaleimide, to avoid post-mortem calpain overactivation. The injected striata were then dissected and immediately sonicated in radioimmunoprecipitation assay buffer [50 mM Tris–HCl, pH 7.4, 150 mM NaCl, 7 mM EDTA, 1% NP-40 (nonyl phenoxypolyethoxylethanol), 0.1% SDS, 10 μg/ml DTT (dithiothreitol), 1 mM PMSF (phenylmethylsulphonyl fluoride), 200 μg/ml leupeptin, protease inhibitors cocktail]. Equal amounts (30 μg of protein) were resolved on 12% SDS–PAGE and transferred onto PVDF (polyvinylidene fluoride) membranes. Immunoblotting was performed using the monoclonal anti-ataxin 3 antibody (1H9, 1:1000; Chemicon), anti-calpastatin (H300, 1:200; Santa Cruz), anti-calpain-cleaved α-spectrin (Roberts-Lewis *et al*., 1994) (Ab 38, 1:3000) and anti-actin (clone

AC-74, 1:5000; Sigma) or anti-tubulin (clone SAP.4G5, 1:15 000; Sigma). A partition ratio with actin or tubulin was calculated following quantification with Quantity One® 1-D image analysis software version 4.5.

Statistical analysis

Statistical analysis was performed using Student's *t*-test or ANOVA for multiple comparisons. Values of $P < 0.05$ were considered statistically significant.

Results

Inhibition of calpains in a lentiviral mouse model of Machado–Joseph disease reduces the size and number of neuronal intranuclear inclusions of mutant ataxin 3

In order to investigate the role of calpains in the pathogenesis of spinocerebellar ataxia type 3, we overexpressed the calpain inhibitor calpastatin in a lentiviral mouse model of Machado–Joseph disease (Alves *et al*., 2008). Four-week-old mice were co-injected bilaterally in the striatum with lentiviral vectors encoding ATX-3 72Q and AAV vectors encoding GFP (control, left hemisphere) or calpastatin (right hemisphere; Fig. 1) and were sacrificed 8 weeks post-injection. Mice singly injected with calpastatin and GFP were used as a control of AAV transduction. AAV vectors mediate a delayed expression of calpastatin, when compared with a quicker onset of ataxin 3 expression upon lentiviral transduction, due to the necessity of conversion of the single-stranded genome into double stranded DNA, especially in non-dividing cells (Shevtsova *et al*., 2005). Therefore, co-injection of both viral vectors in the mouse brain allowed cells co-transduction in a phased manner, leading to the development of pathology before maximum expression of the calpain inhibitor 2 weeks later.

Calpain inhibition by calpastatin reduced the size and number of mutant ataxin 3 (ATX-3 72Q) inclusions (Figs 2B, D and K and 4E) when compared to the GFP transduced hemisphere (Figs 2A, C and K and 4E). In this control hemisphere (Fig. 2C) and in cells not infected by calpastatin (Fig. 2D; arrowhead), ATX-3 72Q accumulated in large intranuclear inclusions with 3.98 μm mean diameter and co-localized with ubiquitin (Fig. 2E–G). On the contrary, upon calpastatin overexpression, mutant ataxin 3 inclusions became very small, almost undetectable by fluorescence immunohistochemistry (Fig. 2D), and ubiquitin pattern was diffuse (Fig. 2H–J). Calpain inhibition promoted a 2.9-fold reduction in inclusions diameter to 1.4 μm (Figs 2C and D and 4E) and reduced to 47% the number of N-terminal ataxin 3 inclusions detected with an anti-myc antibody (Fig. 2A, B and K), an effect that was less prominent when inclusions were counted in brightfield upon imunohistochemistry with the 1H9 (recognizes amino acids 221–224) or anti-ubiquitin antibodies (data not shown). This may be due to the fact that the C-terminal of ataxin 3, including the polyglutamine tract, is more prone to aggregation.

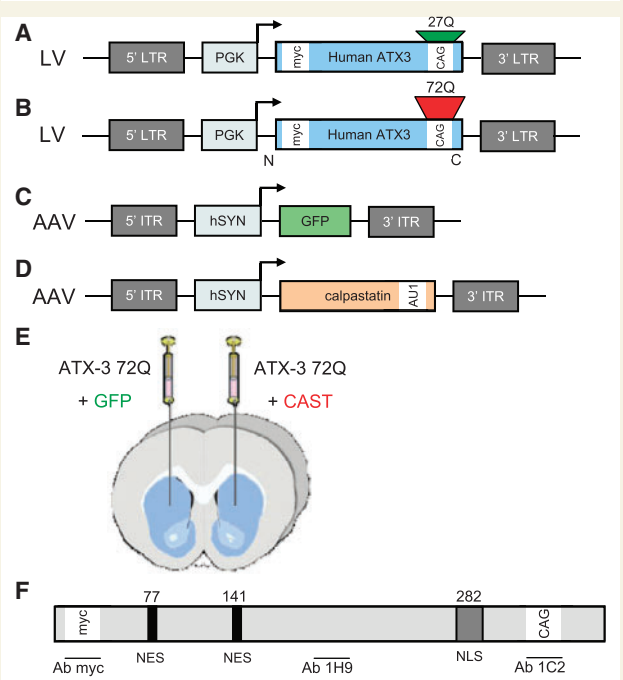

Figure 1 Strategy used to generate an *in vivo* mouse model of Machado–Joseph disease and to inhibit mutant ataxin 3 proteolysis by calpains. Schematic representation of the lentiviral (LV) constructs used in the development of the mouse model of Machado–Joseph disease. Complementary DNAs encoding (**A**) wild-type (27 CAG repeats) or (**B**), mutant ataxin 3 (72 CAG repeats) were cloned in the SIN-W transfer vector. (**C**) Schematic of the AAV1/2 encoding GFP. (**D**) The complementary DNA encoding calpastatin was inserted into an AAV serotype 2 backbone, under the control of the human synapsin 1 gene promoter, which restrains expression to neurons. (**E**) Four-week-old mice were co-injected bilaterally in the striatum with ATX3-72Q and GFP (left hemisphere) or calpastatin (right hemisphere) vectors and were sacrificed 5 and 8 weeks post-injection for western blot and immunohistochemical analysis, respectively (injection co-ordinates: antero-posterior: +0.6 mm; lateral: ±1.8 mm; ventral: −3.5 mm; tooth bar: 0). (**F**) Diagram of ataxin 3 showing antibody recognition sites used in Fig. 5. hSYN = human synapsin 1; ITR = inverted terminal repeat; LTR = long terminal repeat; NES = nuclear export signal; NLS = nuclear localization signal; PGK = phosphoglycerate kinase.

Upon co-infection with vectors encoding wild-type ataxin 3 (ATX-3 27Q) and GFP (left hemisphere) or calpastatin (right hemisphere; Fig. 1), neither ataxin 3 nor ubiquitin inclusions were observed. Furthermore, no difference in the subcellular localization of ATX-3 27Q was observed between the two hemispheres (data not shown).

These results suggest that inhibition of calpain activity in the mouse brain prevents accumulation of mutant ataxin 3 in large intranuclear inclusions.

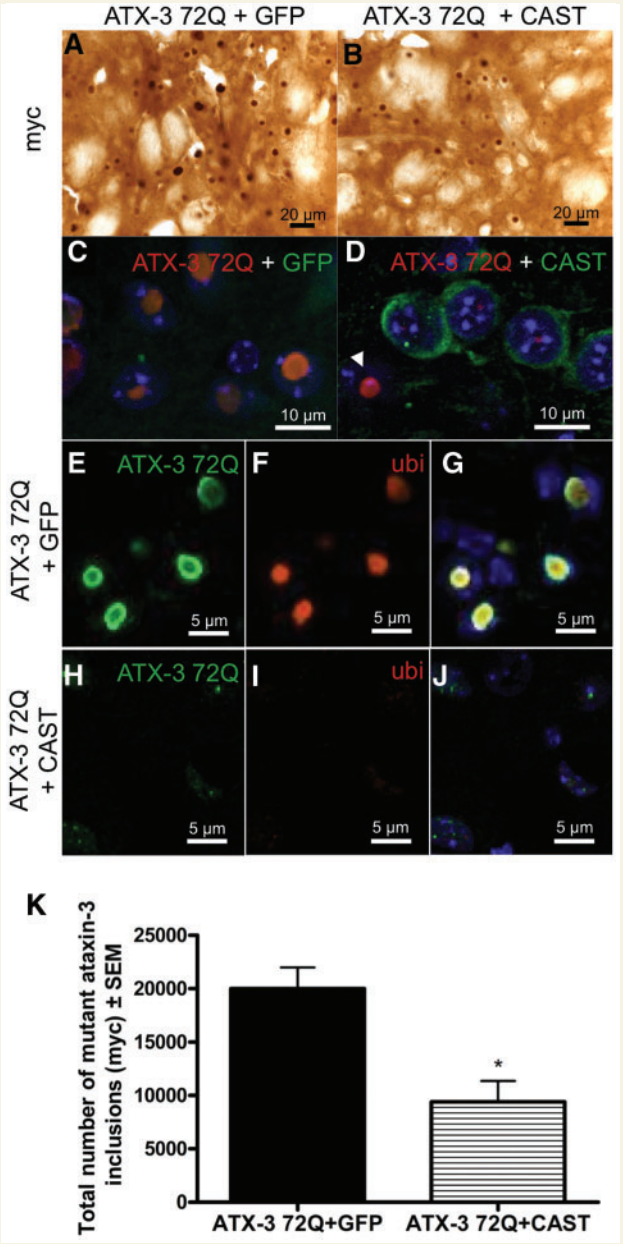

Figure 2 Inhibition of calpains significantly decreases the number of N-terminal mutant ataxin 3 inclusions, while changing mutant ataxin 3 and ubiquitin aggregation pattern. (**A–K**) Co-expression of mutant ataxin 3 and GFP (left hemisphere) or calpastatin (right hemisphere) in the striatum of adult mice, 2 months post-injection. (**A** and **B**) Peroxidase staining using an anti-myc antibody to the myc tag of the N-terminal ataxin 3 (Ab clone 4A6). A significant decrease in the number of N-terminal ataxin 3 inclusions was observed in calpastatin transduced hemisphere. (**C**) Fluorescence staining for mutant ataxin 3 (Ab 1H9, red) localization upon co-expression with GFP (green) or **(D)** calpastatin (Ab H300, green). Nuclear marker (DAPI, blue) was used. As expected, in the GFP transduced hemisphere mutant ataxin 3 was observed as intranuclear inclusions. On the contrary, the cells infected with AAV2-calpastatin showing calpastatin immunoreactivity, presented small inclusions almost not depicted. **(E–G)** Fluorescence staining for co-localization (**G** and **J**) merge of **E** and **F** or **H** and **I** with nuclear marker DAPI (blue) of mutant ataxin 3 (**E** and **H**, Ab 1H9, green) and ubiquitin (**F** and **I**, antibody anti-ubiquitin DAKO, red). While in the control hemisphere mutant ataxin 3 intranuclear inclusions (**E**) were ubiquitinated (**F**) particularly within the central core, (**H–J**) ubiquitin pattern upon calpastatin overexpression was rather diffuse. (**K**) Quantification of the absolute number of myc-positive cells, graph related to panels (**A** and **B**). Statistical significance was evaluated with Student's *t*-test ($n = 4$, $^*P = 0.05$).
SEM = standard error of the mean, CAST = calpastatin.

Inhibition of calpains in a lentiviral mouse model of Machado–Joseph disease mediates striatal neuroprotection

To monitor the effects of calpastatin overexpression over neuronal dysfunction induced by mutant ataxin 3 we performed an immunohistochemical analysis for DARPP-32, a regulator of dopamine receptor signalling (Greengard *et al.*, 1999) which we have previously shown to be downregulated in the striatum of lentiviral and transgenic Machado–Joseph disease animal models (Alves *et al.*, 2008). Loss of DARPP-32 immunoreactivity in the calpastatin injected striatal hemisphere was reduced to 39% when compared with the GFP transduced hemisphere (Fig. 3A–D and G), whereas no loss of DARPP-32 staining was detected in mice co-injected with ATX-3 27Q and GFP or calpastatin (data not shown). This is indicative of a neuroprotective effect provided by the selective inhibition of calpains.

Additionally, cresyl violet-stained sections further demonstrated a significant reduction in the number of shrunken hyperchromatic nuclei upon calpastatin overexpression (Fig. 3E, F and H), indicating that calpain inhibition prevents cell injury and striatal degeneration induced by mutant ataxin 3 expression in the brain of adult mice.

Calpastatin prevents nuclear translocation of mutant ataxin 3 in a dose-dependent manner

We further assessed the involvement of calpains in the pathogenesis of Machado–Joseph disease by expressing mutant ataxin 3 in the mouse striatum upon three progressively increasing levels of calpastatin (Fig. 4), as follows: (i) wild-type animals; (ii) transgenic mice overexpressing calpastatin (Takano *et al.*, 2005) and (iii) animals injected with AAV vectors encoding calpastatin.

The mean diameter of mutant ataxin 3 intranuclear inclusions was reduced to 2.77 µm in transgenic animals (Fig. 4B and E), 1.4-fold smaller than the control, but 2-fold larger than the mean inclusion size when calpastatin levels were achieved by viral transduction (Fig. 4C and E). Fig. 4D shows the increasing calpastatin protein levels in transgenic mice overexpressing calpastatin and AAV2-calpastatin injected mice.

These results suggest that a critical concentration of calpastatin is necessary to completely inhibit calpain activity in order to prevent mutant ataxin 3 translocation to the nucleus and aggregation.

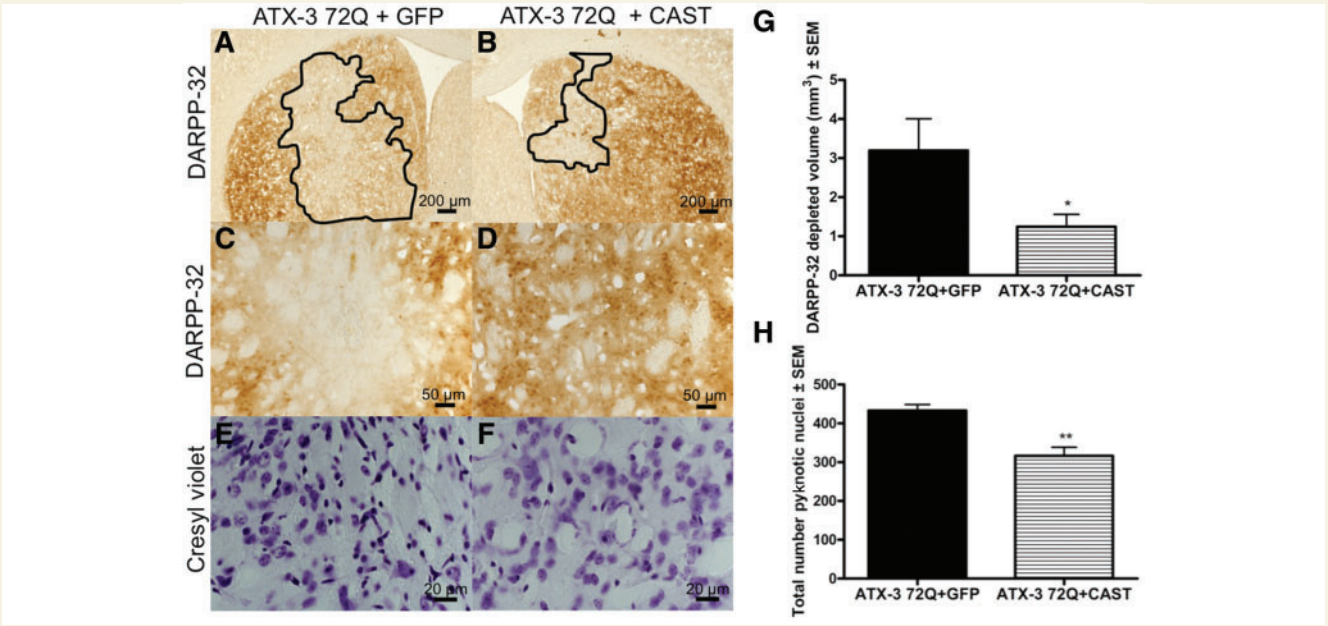

Figure 3 Inhibition of calpains prevents cell injury and striatal degeneration. (**A–H**) Co-expression of mutant ataxin 3 (ATX-3 72Q) and GFP (left hemisphere) or calpastatin (CAST, right hemisphere) in the striatum of adult mice, 2 months post-injection. (**A–D**) Peroxidase staining using an anti-DARPP-32 antibody. (**C** and **D**) Higher magnification of **A** and **B**. (**A** and **C**) A major loss of DARPP-32 immunoreactivity was observed in the striatum infected with ATX-3 72Q and GFP (**B** and **D**), whereas minor DARPP-32 loss was observed in the striatum infected with ATX-3 72Q and calpastatin. (**E** and **F**) Cresyl violet staining of (**E**) ATX-3 72Q + GFP and (**F**) ATX-3 72Q + calpastatin transduced hemispheres of adult mice. (**G**) Quantification analysis of the DARPP-32-depleted region in the brains of mice. The lesion volume in the hemisphere infected with ATX-3 72Q and calpastatin was much smaller than that in the hemisphere infected with ATX3-72Q and GFP, indicative of a neuroprotective effect conferred by the inhibition of calpains ($n = 4$, $^{*}P = 0.05$). (**H**) Quantification analysis of the pyknotic nuclei visible in both hemispheres on cresyl violet-stained sections. More pyknotic nuclei were visible in the GFP transduced hemisphere, suggesting that calpastatin prevented cell injury and striatal degeneration after co-injection with ATX-3 72Q. All the pictures were taken around the injection site area and show representative immunohistochemical stainings. Statistical significance was evaluated with Student's *t*-test ($n = 4$, $^{**}P < 0.01$). SEM = standard error of the mean.

Inhibition of calpains reduces ataxin 3 proteolysis

To investigate the mechanism by which calpain inhibition modified the subcellular localization of mutant ataxin 3, thereby preventing its nuclear localization, neuronal dysfunction and neurodegeneration, we performed western blot analysis of brain punches of mice subjected to the previously described experimental paradigm (Fig. 1E) but sacrificed at an earlier time point: 5 weeks post-injection. Striatal punches of non-injected and ATX-3 27Q transduced hemispheres were used as controls. Importantly, two ataxin 3 fragments of ~26 and ~34 kDa were strongly detected in the brain hemispheres expressing mutant ataxin 3 (Fig. 5A; arrowheads), but sparingly and not detected, respectively, in those overexpressing wild-type and only expressing endogenous ataxin 3 (Fig. 5D); thus confirming *in vivo* that mutant ataxin 3 is cleaved into fragments that accumulate in the brain and that a wild-type fragment may be more rapidly degraded. Notably, inhibition of calpains activity, confirmed by a decreased immunolabelling of calpain-cleaved α-spectrin (Ab 38; Fig. 5E), a natural substrate of calpains, decreased by 39% the production of the ~26 kDa mutant ataxin 3 fragment (Fig. 5A and F), which was also detected using a N-terminal antibody (Ab myc; Fig. 5C) and a C-terminal antibody specific for the polyglutamine stretch (Ab 1C2; Fig. 5B). In addition, the formation of the ~34 kDa fragment was also decreased by 17%, being this fragment only C-terminal and only generated from the mutant protein (Fig. 5G).

These results are in accordance with the 'toxic fragment hypothesis' and strongly support the idea that inhibition of ataxin 3 cleavage by calpains may be the basis of the calpastatin neuroprotective mechanism.

Calpastatin is depleted from cells with mutant ataxin 3 intranuclear inclusions

Progression of Machado–Joseph disease could be propelled by depletion of calpastatin, which would accelerate calpains dysregulation and lead to neurodegeneration. To investigate this hypothesis, we evaluated the immunoreactivity for calpastatin upon expression of mutant ataxin 3 in the previously described calpastatin transgenic mice (Takano *et al*., 2005). Whereas a strong calpastatin immunoreactivity was observed in the hemisphere transduced with lentiviral vectors encoding ATX-3 27Q, a significant reduction of calpastatin immunostaining by 18%, was observed in cells

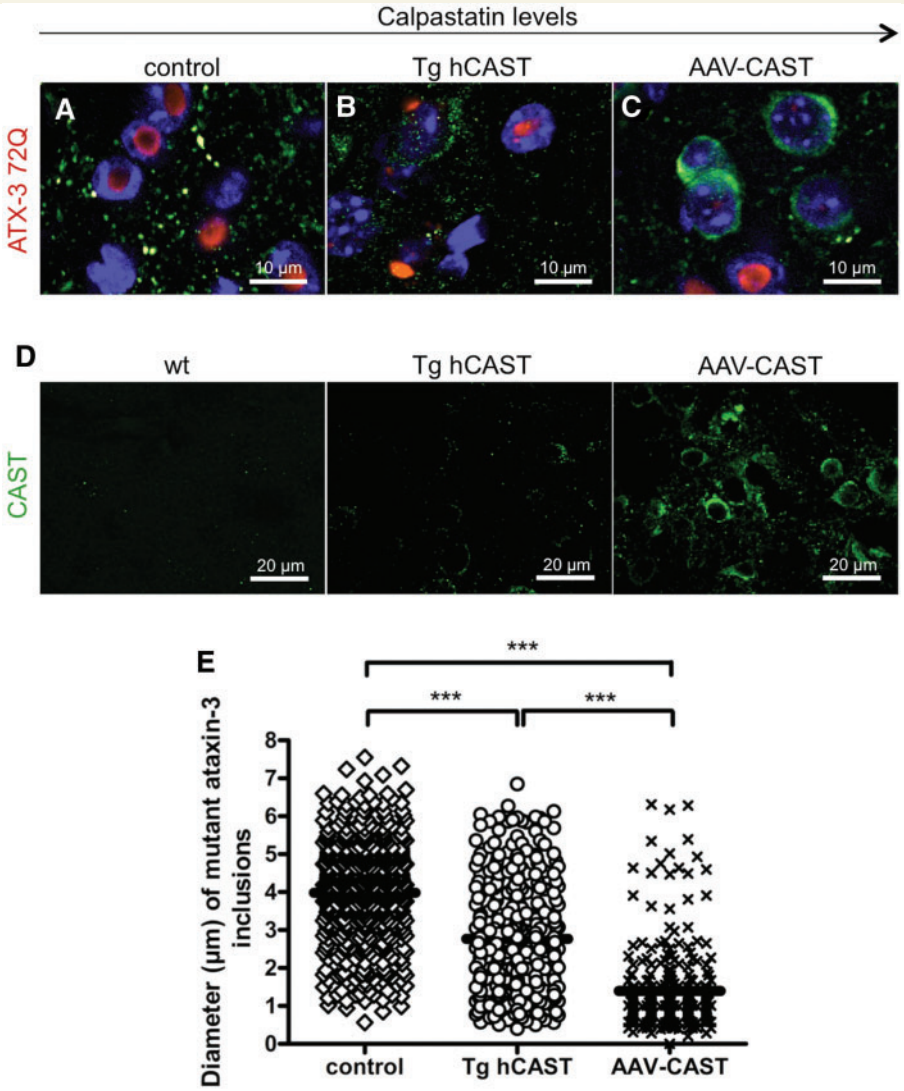

Figure 4 Inhibition of calpains prevents nuclear translocation and aggregation of mutant ATX-3 in a dose dependent manner. Subcellular localization of mutant ataxin 3 (ATX-3 72Q, Ab 1H9, red) when co-injected with GFP (green, $n = 4$; **A**), in transgenic mice overexpressing calpastatin (Tg hCAST, $n = 8$; **B**) and when co-injected with calpastatin (CAST, Ab H300, green, $n = 4$; **C** and **D**). Nuclear marker (DAPI, blue) was used. As the levels of calpastatin increased (**A** to **B** and **B** to **C**), aggregation in the nucleus was prevented. (**D**) Calpastatin immunoreactivity (CAST, Ab H300, green) is lower in wild-type (wt) and transgenic mice overexpressing calpastatin (Tg hCAST) than in AAV-2 calpastatin injected mice. (**E**) Analysis of inclusion diameters showing double staining for mutant ataxin 3 with Ab 1H9 and GFP or calpastatin (***$P < 0.0001$).

where mutant ataxin 3 inclusions were present (Fig. 6A–F and J). Interestingly, in Fig. 6F, the cell highlighted with an arrow, where no ataxin 3 inclusions were observed, presented a similar calpastatin immunolabeling to those transduced with ATX3 27Q, contrasting with the reduced immunostaining detected in the cells pointed with arrowheads with large ataxin 3 intranuclear inclusions.

Calpastatin depletion was further confirmed by immunoblot analysis of brains from calpastatin transgenic mice (Fig. 6G and K). Calpastatin levels were reduced by 26% in the hemisphere where mutant ataxin 3 was overexpressed in comparison to the contra-lateral hemisphere with wild-type ataxin 3 overexpression.

To validate calpastatin depletion in Machado–Joseph disease we analysed calpastatin levels in patient post-mortem tissue and in a transgenic mouse model of the disease using western blot (Torashima *et al.*, 2008; Oue *et al.*, 2009). A dramatic 68% reduction of calpastatin levels was found in the transgenic mouse model, when compared with wild-type mice (Fig. 6H and L). Importantly, in human tissue we observed that calpastatin levels were reduced by 67, 25 and 7% in samples from dentate nucleus of three patients with Machado–Joseph disease compared with the control (Fig. 6I and M).

These results indicate that upon mutant ataxin 3 expression, calpastatin is depleted, which may in turn increase calpain activity, ataxin 3 proteolysis, nuclear translocation, aggregation and toxicity, ultimately triggering or at least severely aggravating the pathogenesis of Machado–Joseph disease.

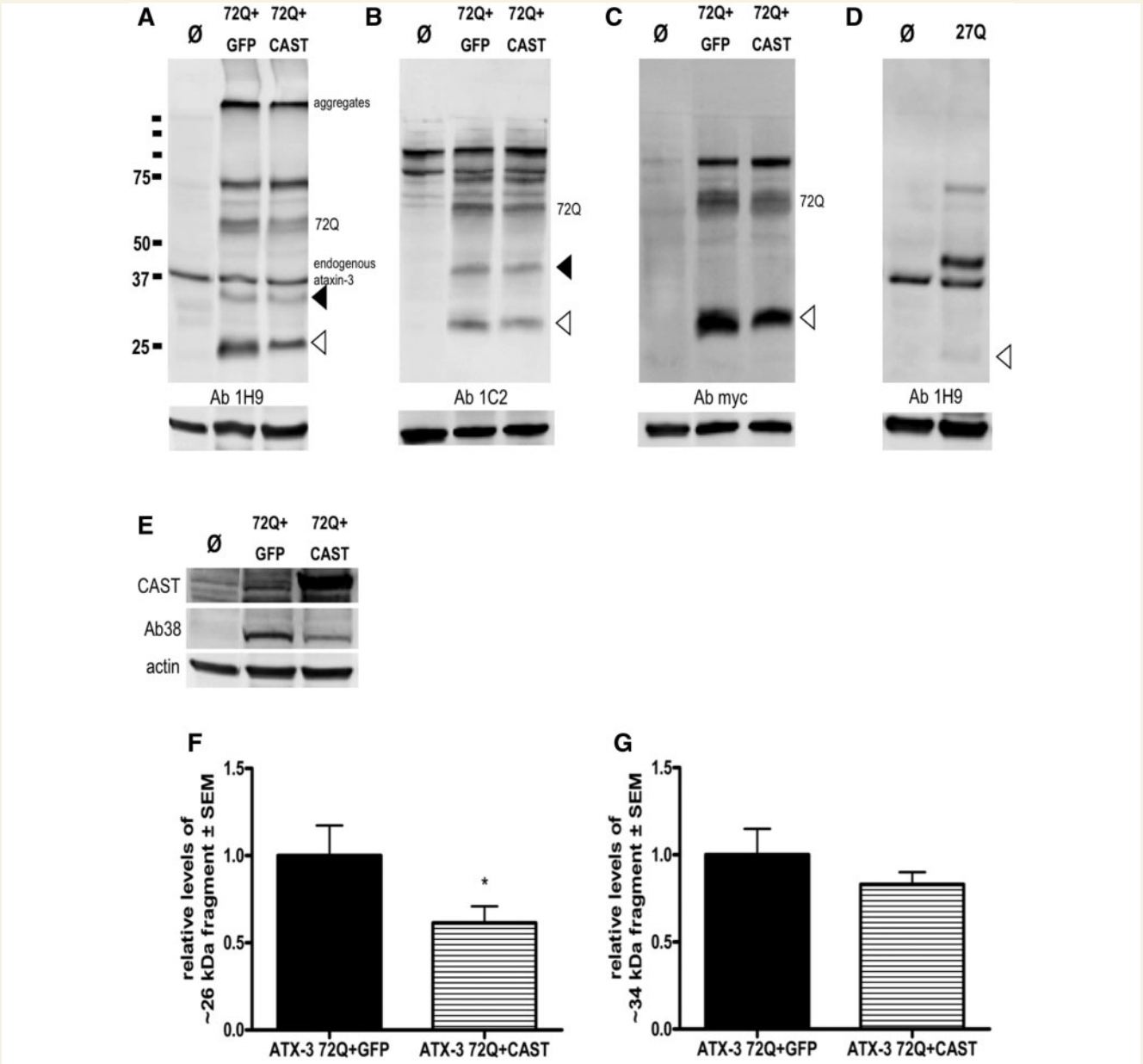

Figure 5 Ataxin 3 proteolysis in the lentiviral mouse model of Machado–Joseph disease is decreased upon calpastatin overexpression. At 5 weeks post-injection, mice ($n = 7$) co-injected bilaterally with mutant ataxin 3 (ataxin 3 72Q) and GFP (left hemisphere) or calpastatin (CAST, right hemisphere) were sacrificed and punches of the striatum were made to perform a western blot analysis with several antibodies to detect different epitopes of ataxin 3 protein: (**A**) Ab 1H9, which recognizes amino acids E214-L233; (**B**) Ab 1C2, specific for the polyglutamine stretch, present at the C-terminal of ataxin 3; and (**C**) Ab myc, which recognizes the myc tag located at the N-terminal of mutant ataxin 3. Two fragments of ~26 and ~34 kDa were detected (empty and shaded arrowheads, respectively). (**D**) Striatal punches of non-injected and ataxin 3 27Q transduced hemispheres. (**E**) Levels of calpastatin (CAST, antibody H300) and of calpain-cleaved α-spectrin (antibody 38) are also shown. (**F** and **G**) Densitometric quantification of ~26 and ~34 kDa fragments levels of mutant ataxin 3 relative to actin, shown in panel **A** ($n = 7$, $^*P = 0.05$). The ~26 kDa fragment is clearly detected by Ab 1H9, Ab 1C2 and anti-myc in the mutant ataxin 3 sample, but faintly in the transgenic wild-type and not detected in the endogenous ataxin 3 sample. The ~34 kDa fragment is only detected in the mutant ataxin 3 sample using Ab 1H9 and Ab 1C2. SEM = standard error of the mean.

Discussion

In this work, we provide *in vivo* evidence that calpains are proteolytic enzymes involved in the pathogenesis of Machado–Joseph disease and that inhibition of calpains reduces cleavage of mutant ataxin 3, its translocation to the nucleus, aggregation in nuclear inclusions, neurotoxicity and neurodegeneration.

The neurotoxicity associated with Machado–Joseph disease has been proposed to be derived from a mutant ataxin 3 cleavage

fragment (Ikeda *et al*., 1996; Haacke *et al*., 2006; Takahashi *et al*., 2008; Koch *et al*., 2011), which above a critical concentration becomes cytotoxic (Goti *et al*., 2004). Based on cell or *in vitro* models, mutant ataxin 3 has been reported to be a substrate for caspases (Berke *et al*., 2004; Jung *et al*., 2009), subject to autolytic cleavage (Mauri *et al*., 2006) and a substrate for calpains (Haacke *et al*., 2007; Koch *et al*., 2011). An additional cleavage site was proposed in a mouse model, within the N-terminus of amino acid 190, which might be neither a caspase nor a calpain product (Colomer Gould *et al*., 2007).

To clarify this issue, we overexpressed the endogenous calpain-specific inhibitor calpastatin in a lentiviral mouse model of Machado–Joseph disease and used transgenic mice overexpressing calpastatin (Takano *et al*., 2005). This approach overcomes the use of synthetic peptidic, peptide-mimetic and non-peptidic calpain inhibitors currently available, which have problems of specificity, metabolic stability, water-solubility and/or penetration through the blood–brain barrier (Higuchi *et al*., 2005). Instead of using the lentiviral model in the rat (Alves *et al*., 2008), here we generated an analogous model in C57BL/6J mice that allows comparison of results with those obtained in the transgenic mice overexpressing calpastatin, and to previous *in vivo* studies.

As expected, upon mutant ataxin 3 expression, the expanded protein accumulated as intranuclear inclusions co-localizing with ubiquitin in the mouse brain (Fig. 2C and E–G). A marked loss of DARPP-32 immunoreactivity and a large number of pyknotic nuclei were observed (Fig. 3), suggesting cell injury and neurodegeneration. In contrast, when mutant ataxin 3 was co-injected with calpastatin to specifically inhibit calpains, a robust and dose-dependent decrease in the size and number of C- and N-terminal ataxin 3 inclusions, respectively, (Fig. 2A, B and K) was observed. In addition, the volume of the region depleted of DARPP-32 immunoreactivity and the number of pyknotic nuclei were significantly and robustly decreased (Fig. 3), indicating that calpain inhibition prevents cell injury and provides neuroprotection.

Cleavage fragments of mutant ataxin 3, whose existence has been controversial, were clearly detected *in vivo* in this study. While we were finalizing this work, a study in patient-specific induced pluripotent stem cell-derived neurons also reported the formation of cleavage fragments of mutant ataxin 3 upon L-glutamate or NMDA (*N*-methyl-D-aspartate) stimulus (Koch *et al*., 2011). The two studies are concordant on providing compelling evidence of the involvement of calpains in Machado–Joseph disease, but not on the trigger for calpain activation, as in our study, cleavage of mutant ataxin 3 occurred without overstimulation of glutamate receptors.

Cleavage of mutant ataxin 3 (Fig. 5) might occur at amino acid 220 (Fig. 1), giving rise to two different fragments of similar molecular weight detected by Ab 1H9 (Fig. 5A), which recognizes the human ataxin 3 fragment from amino acids E214-L233, Ab myc (Fig. 5C), an antibody for a myc tag located at the N-terminal of the protein and Ab 1C2 (Fig. 5B), an antibody specific for the polyglutamine stretch, present at ataxin 3 C-terminal (Fig. 1F). A simultaneous cleavage at amino acids 60 and 260 proposed by Haacke *et al*. (2007) may lead to the final ~26 kDa fragment, detected by Ab 1H9. Cleavage at amino acid 154 may generate a mutant C-terminal ~34 kDa fragment only detected by Ab 1H9 (Fig. 5A) and Ab 1C2 (Fig. 5B), but not by Ab myc (Fig. 5C).

These results support the toxic fragment hypothesis indicating that calpastatin promotes neuroprotection by decreasing mutant ataxin 3 fragment production, suggesting that the pathogenesis of Machado–Joseph disease is strongly associated with mutant ataxin 3 proteolysis by calpains. As evidenced by the decreased cleavage of α-spectrin, a potential biomarker for neuronal cell injury (Liu *et al*., 2008) and ataxin 3 (Fig. 5A and E), upon calpastatin overexpression, proteolysis of other substrates might also be inhibited as well as other functions regulated by calpains under pathological conditions not addressed in our studies. Recent evidences suggest that not only the C-terminal fragment is cytotoxic (Ikeda *et al*., 1996; Goti *et al*., 2004), but that the non-polyglutamine containing ataxin 3 N-terminus fragment is also toxic and may contribute to an impaired unfolded protein response in the pathogenesis of Machado–Joseph disease (Hubener *et al*., 2011). Our results show that calpastatin overexpression leads to a decrease of both fragments formation. Further evidence that calpastatin exerted neuroprotection may also be drawn from the subcellular localization of the ataxin 3 species.

Ataxin 3, when non-expanded, is enriched in the cytoplasm (Paulson *et al*., 1997*a*; Schmidt *et al*., 1998; Goti *et al*., 2004), but upon polyglutamine expansion the protein accumulates in the nucleus. This nuclear localization is required for the *in vivo* manifestation of Machado–Joseph disease neuropathology. Accordingly, transgenic mice with 148 CAGs but attached to a nuclear export signal only develop a milder phenotype with few inclusions (Bichelmeier *et al*., 2007). However, how ataxin 3 enters the nucleus under pathogenic conditions and forms aggregates is a matter of debate. It has been proposed that CK2-dependent phosphorylation determines cellular localization (Mueller *et al*., 2009) and that proteotoxic stress increases nuclear localization of ataxin 3 (Reina *et al*., 2010), while other reports underline the importance of nuclear localization (NLS282) and nuclear export (NES 77 and 141) signals to ataxin 3 intracellular localization (Antony *et al*., 2009; Macedo-Ribeiro *et al*., 2009). Accordingly, we found that the number of inclusions detected with the antibody targeting the N-terminal ataxin 3 was significantly lower than the amount found when using the 1H9 antibody (amino acids 221–224) in both GFP and calpastatin-transduced hemispheres. This suggests that the C-terminal fragment, including the nuclear localization signal and the polyglutamine stretch, is more prone to aggregation and accumulates in higher extension in the nucleus as compared to the N-terminal fragment carrying the nuclear export signal sequences (Schmidt *et al*., 1998; Goti *et al*., 2004; Koch *et al*., 2011; Walsh *et al*., 2005). Furthermore, our results show that proteolysis of mutant ataxin 3 by calpains is required for its translocation to the nucleus in a dose-dependent manner (Fig. 4). As calpastatin levels increase, the diameter of mutant ataxin 3 inclusions progressively decreases (Fig. 4A: 3.98 μm; B: 2.77 μm; and C: 1.40 μm). Our results suggest that calpains cleavage between the nuclear export signals and the nuclear localization signal discussed above may account for the enhanced transport of the

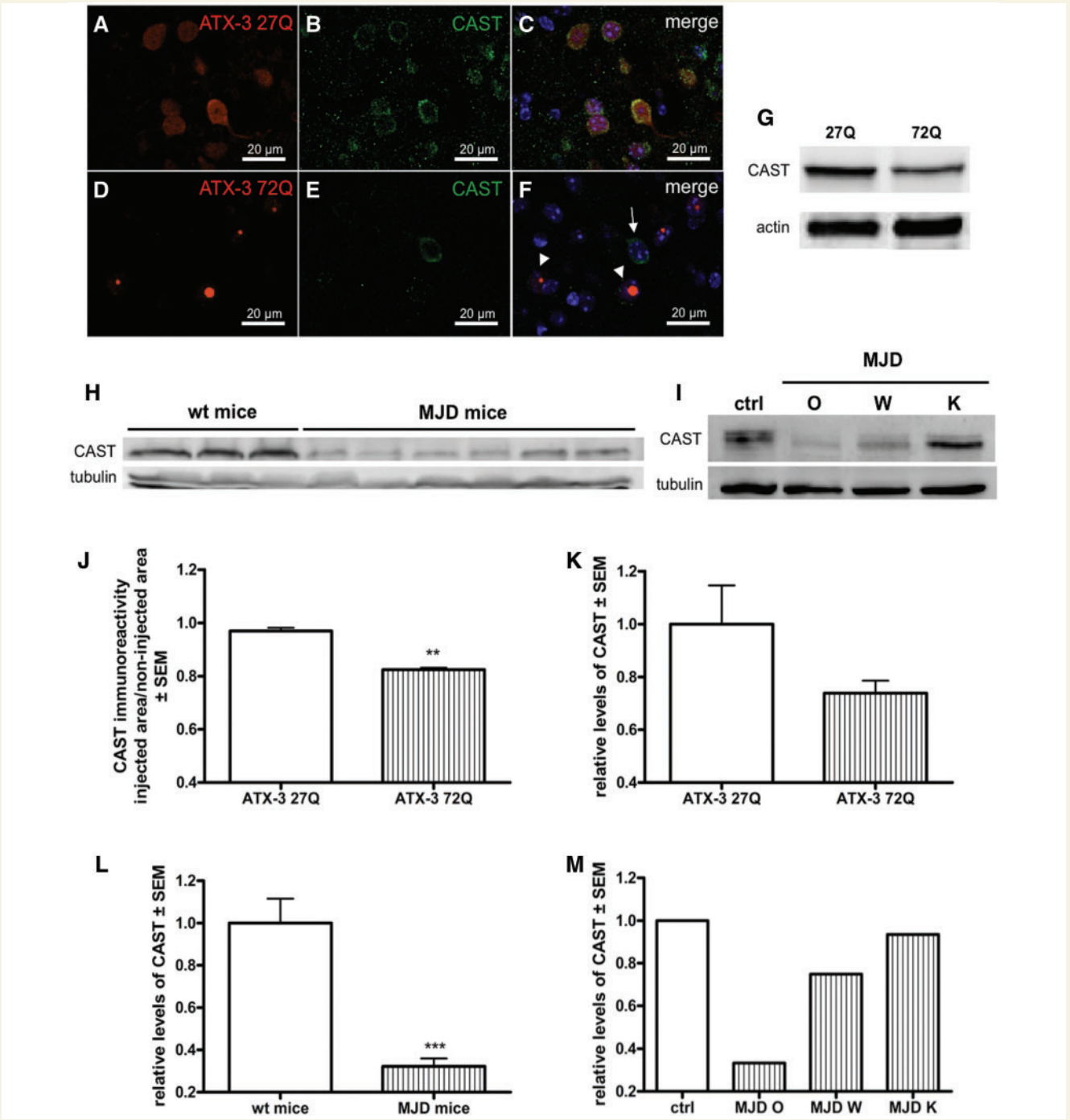

Figure 6 Calpastatin is depleted from cells with mutant ataxin 3 intranuclear inclusions. Transgenic mice overexpressing calpastatin (Tg hCAST) were injected bilaterally: wild-type ataxin 3 (ataxin 3 27Q) in the left hemisphere and mutant ataxin 3 (ataxin 3 72Q) in the right hemisphere and were sacrificed 4 weeks post-injection for (**A**-**F**,**J**), immunohistochemistry and (**G**,**K**), western blot analysis ($n = 6$; **H**). (**A–F**) Fluorescence staining for ataxin 3 (Ab 1H9, red; **A** and **D**), and in **B** and **E**, calpastatin (CAST, Ab H300, green) and nuclear marker (DAPI, blue). (**A–C**) While cells infected with ataxin 3 27Q presented a strong calpastatin immunoreactivity, when ataxin 3 72Q was injected (**D–F**), the cells in which intranuclear inclusions were present showed nearly no calpastatin immunolabelling. (**F**) Even in the same hemisphere, in opposition to the cell indicated with an arrow, the cells with intranuclear inclusions (indicated with arrow heads) did not overexpress calpastatin, suggesting that the endogenous calpain inhibitor was depleted upon mutant ataxin 3 expression. Western blot analysis with anti-calpastatin antibody (Ab H300) revealed a decrease of calpastatin levels in mutant ataxin 3 transduced hemisphere compared with its contralateral hemisphere (**G**); and also in lysates obtained from dissected cerebella of a Machado–Joseph disease transgenic mouse model ($n = 5$; **H**) and from dentate nucleus of Patients O, W and K with Machado–Joseph disease (**I**). (**J**) Quantitative analysis of calpastatin immunoreactivity ($n = 4$, $^{**}P < 0.01$). (**K–M**) Densitometric quantification of calpastatin levels, shown in panels **G–I**, respectively. MJD = Machado–Joseph disease; SEM = standard error of the mean.

C-terminal fragment simultaneously carrying the nuclear localization signal and the expanded polyglutamine tract of ataxin 3 from the cytoplasm to the nucleus. Altogether, calpain activity is required for mutant ataxin 3 translocation to the nucleus, and this effect is antagonized by the presence of calpastatin.

Finally, our studies suggest that upon mutant ataxin 3 expression calpastatin is depleted (Fig. 6), in accordance to what was observed in models of Alzheimer's disease, where the progression is propelled by a marked depletion of calpastatin, upstream of calpain activation (Rao *et al*., 2008). Calpastatin depletion was observed not only in the lentiviral mouse model, but also in a mouse model of Machado–Joseph disease (Torashima *et al*., 2008; Oue *et al*., 2009) and in human brain tissue. Rather than simply its consequence, we speculate that calpastatin depletion may progressively lead to calpain overactivation. Our results suggest that calpain activation promotes mutant ataxin 3 cleavage, which in turn translocates to the nucleus and aggregates, and that during this process calpastatin might also be cleaved, further contributing to calpain overactivation. This observation may also explain the larger diameter of mutant ataxin 3 inclusions in transgenic mice overexpressing calpastatin than in mice infected with AAV2-calpastatin (Fig. 4). In this experiment, lower calpastatin overexpression levels may have been insufficient to overcome calpastatin depletion, and to inhibit and prevent nuclear aggregation.

In conclusion, we established the connection *in vivo* between mutant ataxin 3 proteolysis by calpains, fragment production and nuclear localization, which contributes to the elucidation of the pathogenic mechanism of Machado–Joseph disease. Furthermore, we show that calpastatin, the endogenous calpain-specific inhibitor, is able to block this mechanism, preventing nuclear translocation of mutant ataxin 3, consequent aggregation and nuclear toxicity. Therefore, these findings indicate that calpains are promising targets for therapeutic intervention in Machado–Joseph disease.

Acknowledgements

The authors thank Dr Luísa Cortes for expert technical assistance with confocal microscopy, Dr Takaomi Saido for providing the calpastatin transgenic animals, Dr Robert Siman for providing the antibody to calpain-cleaved α-spectrin (Ab 38) and Dr Hirokazu Hirai for providing the transgenic Machado–Joseph disease mouse model.

Funding

This work was funded by The Portuguese Foundation for Science and Technology, references PTDC/SAU-NEU/099307/2008, The Richard Chin and Lilly Lock Research Fund, Association Française de Myopathies (AFM) and the National Ataxia Foundation (NAF). Ana Teresa Simões and Nélio Gonçalves were supported by the Portuguese Foundation for Science and Technology, Fellowships SFRH/BD/33186/2007 and SFRH/BD/38636/2007.

References

Alves S, Regulier E, Nascimento-Ferreira I, Hassig R, Dufour N, Koeppen A, et al. Striatal and nigral pathology in a lentiviral rat model of Machado–Joseph disease. Hum Mol Genet 2008; 17: 2071–83.

Antony PM, Mantele S, Mollenkopf P, Boy J, Kehlenbach RH, Riess O, et al. Identification and functional dissection of localization signals within ataxin-3. Neurobiol Dis 2009; 36: 280–92.

Berke SJ, Schmied FA, Brunt ER, Ellerby LM, Paulson HL. Caspase-mediated proteolysis of the polyglutamine disease protein ataxin-3. J Neurochem 2004; 89: 908–18.

Bichelmeier U, Schmidt T, Hubener J, Boy J, Ruttiger L, Habig K, et al. Nuclear localization of ataxin-3 is required for the manifestation of symptoms in SCA3: *in vivo* evidence. J Neurosci 2007; 27: 7418–28.

Breuer P, Haacke A, Evert BO, Wullner U. Nuclear aggregation of polyglutamine-expanded ataxin-3: fragments escape the cytoplasmic quality control. J Biol Chem 2010; 285: 6532–7.

Burnett B, Li F, Pittman RN. The polyglutamine neurodegenerative protein ataxin-3 binds polyubiquitylated proteins and has ubiquitin protease activity. Hum Mol Genet 2003; 12: 3195–205.

Chai Y, Berke SS, Cohen RE, Paulson HL. Poly-ubiquitin binding by the polyglutamine disease protein ataxin-3 links its normal function to protein surveillance pathways. J Biol Chem 2004; 279: 3605–11.

Colomer Gould VF, Goti D, Pearce D, Gonzalez GA, Gao H, Bermudez de Leon M, et al. A mutant ataxin-3 fragment results from processing at a site N-terminal to amino acid 190 in brain of Machado–Joseph disease-like transgenic mice. Neurobiol Dis 2007; 27: 362–9.

de Almeida LP, Ross CA, Zala D, Aebischer P, Deglon N. Lentiviral-mediated delivery of mutant huntingtin in the striatum of rats induces a selective neuropathology modulated by polyglutamine repeat size, huntingtin expression levels, and protein length. J Neurosci 2002; 22: 3473–83.

de Almeida LP, Zala D, Aebischer P, Deglon N. Neuroprotective effect of a CNTF-expressing lentiviral vector in the quinolinic acid rat model of Huntington's disease. Neurobiol Dis 2001; 8: 433–46.

Doss-Pepe EW, Stenroos ES, Johnson WG, Madura K. Ataxin-3 interactions with rad23 and valosin-containing protein and its associations with ubiquitin chains and the proteasome are consistent with a role in ubiquitin-mediated proteolysis. Mol Cell Biol 2003; 23: 6469–83.

Goti D, Katzen SM, Mez J, Kurtis N, Kiluk J, Ben-Haiem L, et al. A mutant ataxin-3 putative-cleavage fragment in brains of Machado–Joseph disease patients and transgenic mice is cytotoxic above a critical concentration. J Neurosci 2004; 24: 10266–79.

Greengard P, Allen PB, Nairn AC. Beyond the dopamine receptor: the DARPP-32/protein phosphatase-1 cascade. Neuron 1999; 23: 435–47.

Haacke A, Broadley SA, Boteva R, Tzvetkov N, Hartl FU, Breuer P. Proteolytic cleavage of polyglutamine-expanded ataxin-3 is critical for aggregation and sequestration of non-expanded ataxin-3. Hum Mol Genet 2006; 15: 555–68.

Haacke A, Hartl FU, Breuer P. Calpain inhibition is sufficient to suppress aggregation of polyglutamine-expanded ataxin-3. J Biol Chem 2007; 282: 18851–6.

Higuchi M, Tomioka M, Takano J, Shirotani K, Iwata N, Masumoto H, et al. Distinct mechanistic roles of calpain and caspase activation in neurodegeneration as revealed in mice overexpressing their specific inhibitors. J Biol Chem 2005; 280: 15229–37.

Hubener J, Vauti F, Funke C, Wolburg H, Ye Y, Schmidt T, et al. N-terminal ataxin-3 causes neurological symptoms with inclusions, endoplasmic reticulum stress and ribosomal dislocation. Brain 2011; 134: 1925–42.

Ikeda H, Yamaguchi M, Sugai S, Aze Y, Narumiya S, Kakizuka A. Expanded polyglutamine in the Machado–Joseph disease protein induces cell death in vitro and in vivo. Nat Genet 1996; 13: 196–202.

Jung J, Xu K, Lessing D, Bonini NM. Preventing Ataxin-3 protein cleavage mitigates degeneration in a Drosophila model of SCA3. Hum Mol Genet 2009; 18: 4843–52.

Kawaguchi Y, Okamoto T, Taniwaki M, Aizawa M, Inoue M, Katayama S, et al. CAG expansions in a novel gene for Machado–Joseph disease at chromosome 14q32.1. Nat Genet 1994; 8: 221–8.

Koch P, Breuer P, Peitz M, Jungverdorben J, Kesavan J, Poppe D, et al. Excitation-induced ataxin-3 aggregation in neurons from patients with Machado–Joseph disease. Nature 2011; 480: 543–6.

Kugler S, Lingor P, Scholl U, Zolotukhin S, Bahr M. Differential transgene expression in brain cells in vivo and in vitro from AAV-2 vectors with small transcriptional control units. Virology 2003; 311: 89–95.

Liu J, Liu MC, Wang KK. Calpain in the CNS: from synaptic function to neurotoxicity. Sci Signal 2008; 1: re1.

Macedo-Ribeiro S, Cortes L, Maciel P, Carvalho AL. Nucleocytoplasmic shuttling activity of ataxin-3. PLoS One 2009; 4: e5834.

Marfori M, Mynott A, Ellis JJ, Mehdi AM, Saunders NF, Curmi PM, et al. Molecular basis for specificity of nuclear import and prediction of nuclear localization. Biochim Biophys Acta 2011; 1813: 1562–77.

Mauri PL, Riva M, Ambu D, De Palma A, Secundo F, Benazzi L, et al. Ataxin-3 is subject to autolytic cleavage. FEBS J 2006; 273: 4277–86.

Mueller T, Breuer P, Schmitt I, Walter J, Evert BO, Wullner U. CK2-dependent phosphorylation determines cellular localization and stability of ataxin-3. Hum Mol Genet 2009; 18: 3334–43.

Oue M, Mitsumura K, Torashima T, Koyama C, Yamaguchi H, Furuya N, Hirai H. Characterization of mutant mice that express polyglutamine in cerebellar Purkinje cells. Brain Res 2009; 1255: 9–17.

Paulson HL, Das SS, Crino PB, Perez MK, Patel SC, Gotsdiner D, et al. Machado–Joseph disease gene product is a cytoplasmic protein widely expressed in brain. Ann Neurol 1997a; 41: 453–62.

Paulson HL, Perez MK, Trottier Y, Trojanowski JQ, Subramony SH, Das SS, et al. Intranuclear inclusions of expanded polyglutamine protein in spinocerebellar ataxia type 3. Neuron 1997b; 19: 333–44.

Rao MV, Mohan PS, Peterhoff CM, Yang DS, Schmidt SD, Stavrides PH, et al. Marked calpastatin (CAST) depletion in Alzheimer's disease accelerates cytoskeleton disruption and neurodegeneration: neuroprotection by CAST overexpression. J Neurosci 2008; 28: 12241–54.

Reina CP, Zhong X, Pittman RN. Proteotoxic stress increases nuclear localization of ataxin-3. Hum Mol Genet 2010; 19: 235–49.

Roberts-Lewis JM, Savage MJ, Marcy VR, Pinsker LR, Siman R. Immunolocalization of calpain I-mediated spectrin degradation to vulnerable neurons in the ischemic gerbil brain. J Neurosci 1994; 14: 3934–44.

Rubinsztein DC, Wyttenbach A, Rankin J. Intracellular inclusions, pathological markers in diseases caused by expanded polyglutamine tracts? J Med Genet 1999; 36: 265–70.

Scheel H, Tomiuk S, Hofmann K. Elucidation of ataxin-3 and ataxin-7 function by integrative bioinformatics. Hum Mol Genet 2003; 12: 2845–52.

Schmidt T, Landwehrmeyer GB, Schmitt I, Trottier Y, Auburger G, Laccone F, et al. An isoform of ataxin-3 accumulates in the nucleus of neuronal cells in affected brain regions of SCA3 patients. Brain Pathol 1998; 8: 669–79.

Shevtsova Z, Malik JM, Michel U, Bahr M, Kugler S. Promoters and serotypes: targeting of adeno-associated virus vectors for gene transfer in the rat central nervous system in vitro and in vivo. Exp Physiol 2005; 90: 53–9.

Sudarsky L, Coutinho P. Machado–Joseph disease. Clin Neurosci 1995; 3: 17–22.

Takahashi T, Kikuchi S, Katada S, Nagai Y, Nishizawa M, Onodera O. Soluble polyglutamine oligomers formed prior to inclusion body formation are cytotoxic. Hum Mol Genet 2008; 17: 345–56.

Takano J, Tomioka M, Tsubuki S, Higuchi M, Iwata N, Itohara S, et al. Calpain mediates excitotoxic DNA fragmentation via mitochondrial pathways in adult brains: evidence from calpastatin mutant mice. J Biol Chem 2005; 280: 16175–84.

Torashima T, Koyama C, Iizuka A, Mitsumura K, Takayama K, et al. Lentivector-mediated rescue from cerebellar ataxia in a mouse model of spinocerebellar ataxia. EMBO Rep 2008; 9: 393–399.

Walsh R, Storey E, Stefani D, Kelly L, Turnbull V. The roles of proteolysis and nuclear localisation in the toxicity of the polyglutamine diseases. A review. Neurotox Res 2005; 7: 43–57.

Wang G, Sawai N, Kotliarova S, Kanazawa I, Nukina N. Ataxin-3, the MJD1 gene product, interacts with the two human homologs of yeast DNA repair protein RAD23, HHR23A and HHR23B. Hum Mol Genet 2000; 9: 1795–803.

Zolotukhin S, Byrne BJ, Mason E, Zolotukhin I, Potter M, Chesnut K, et al. Recombinant adeno-associated virus purification using novel methods improves infectious titer and yield. Gene Ther 1999; 6: 973–85.